Ionic Polymer Actuators: Principle, Fabrication and Applications

Yanjie Wang and Takushi Sugino

Additional information is available at the end of the chapter

Abstract

Ionic-polymer based actuators have the advantages of low voltage and power requirements, being easily processable, flexibility, soft action and bio-mimetic activation, which are of considerable interests for applications in biomedical micro-devices and soft robotics. In this chapter, we firstly review the development of ionic polymer actuator and reveal the universal architecture and mechanism of ionic polymer actuators. We then introduce two kinds of typical polymer actuators: ionic polymer-metal composites (IPMC) and bucky gel actuator (BGA), including their basic principle, fabrication process and typical applications. The aim of this chapter is to give some perspectives on IPMC and BGA and provide a way and case in using this actuator for real applications.

Keywords: electroactive polymer, ionic polymer, actuator, carbon nanotube, ionic liquid

1. Introduction

Recently, as one typical electroactive polymers (EAP), ionic polymer actuators have gradually grown into an important smart material, which is mainly composed of the interlayer for mass transfer and conductive layers on both sides similar to the sandwich structure. When applied an electric field, local stress occurs due to the migration of ions bonded solvent molecules toward the electrode layers, which causes one side to swell and another side to shrink, resulting in bending deformation as shown in **Figure 1**. Due to large bending deformation by low driven voltage, much attention has been focused on ionic polymer actuators [1–3].

The origin of ionic polymer actuators can be traced back to the 1990s of last century. Adolf et al. [4] and Oguro et al. [5] introduced the initial prototype patent of ionic polymer actuators
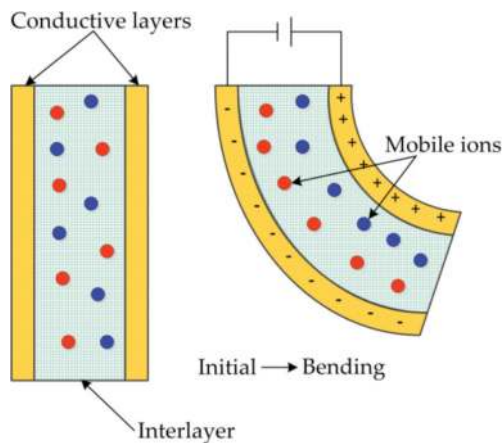
Figure 1. Universal architecture and mechanism of ionic polymer actuators.

in early stage. They both claimed that an actuator comprises an ion exchange membrane and a pair of electrodes attached to opposite surfaces of the ionic polymer, which refers to the cation or anion exchange membrane. Adolf et al. even named the actuator electrically controlled polymeric gel actuators, which maybe is the first normal name of ionic polymer actuator. After that, many researchers were attributed themselves to explore the essential properties of this actuator. They give different names to this special actuator based on different understandings, such as ionic polymeric gel actuator [6], electrically controllable artificial muscle [7], ion-exchange membrane metal composites [8], Nafion-Pt composite actuators (ICPF) [9] and ionic polymer-metal composites (IPMC) [10], which is the most common names so far. At this stage, it is dominant to clarify the actuating mechanism of this kind of actuator. So several electromechanical and physical models were gradually developed by de Gennes et al. [11], Newbury and Leo [12, 13], Nemat-Nasser et al. [14], Tadokoro et al. [9], Zicai Zhu et al. [15, 16] and so on. Meanwhile, for this ionic polymer actuator, the ionomer layer and conductive layer are critical components. The substitutes of components are an important way to improve the electromechanical performance of the actuator. Generally, perfluorinated polymers, such as Nafion (sulfonated) or Flemion (carboxylated), are employed as ionomer layer. The actuation ability of the ionic polymer actuator seriously is dependent on fixed anions, mobile cations and nanochannels inside Nafion or Flemion. Based on this property, a lot of novel hydrocarbon ion-exchangeable membranes are introduced to replace the ionomer layer [2]. These membranes include commercial products, blending and synthetics, some of which overcome the back-reversal problem and show much larger bending deformation compared to the Nafion- or Flemion-IPMC, such as poly(styrene-alt-maleimide) (PSMI)-incorporated poly(vinylidene fluoride) (PVDF) and chitosan/polyaniline interpenetrating polymer network. Likewise, the electrode layer plays an important role in IPMC actuation. It is considered to be easier to modify the electrode layer to optimize the IPMC property than the ionomer layer. Of all metals, gold and platinum with excellent conductivity and chemical stability are the most widely used electrode materials. Because of high cost, inexpensive electrode materials are still in need to replace gold and platinum. Palladium [17], silver [18] or their complex [19] has been considered as substitute.

With the development of new conductive materials, non-metallic materials, such as poly-aniline (PANI), carbon nanotube (CNT) and grapheme etc., are also introduced as electrode materials of the actuator. On this basis, Fukushima et al. [20] proposed a novel kind of fully plastic actuator fabricated by layer-by-layer casting with ionic liquid based bucky gel, which also named bucky-gel actuator (BGA). The bucky-gel actuators composed of the conductive layers of the CNT blending ionic liquid and PVdF(HFP) and the interlayer made of the ionic liquid and PVdF(HFP). In contrast with IPMC, the fabrication process includes neither deposition of metallic layers nor actuating ion exchange. And the bucky-gel actuator can operates stably and quickly in air without back-reversal deformation under DC voltage.

In this chapter, we try to give an overview of two kinds of typical polymer actuators: ionic polymer- metal composites (IPMC) and bucky gel actuator (BGA), including their basic principle, fabrication process and typical applications. We put some results of previous works into more general perspective as well and provide insights of how these results have to be considered for the implementation of future applications. The study and development of polymer actuators are unfolding. This is no doubt that ionic actuators will show great potentials as alternatives for use in the application of precision micro-actuating technology in the future.

2. Principle

As we all know that charged particles will have a directional migration effect when put in the electric field. Generally, parallel plate capacitors would create a uniform electric field between the plates. Special dielectric is added into capacitor, which has unique property with solid–liquid two-phase microstructure. Charged particles (such as cations) do not exist alone in solution environment, and they tend to bind to a certain amount of solvent molecules forming solvated cations. Charged particles together with solvent molecules travel through the liquid-phase microstructure of dielectric from one side to another side when voltage is applied to the plates. This will result in mass plentiful on one side and exhausted on the other side. At this point, mechanical local strain will occur on both sides. These constitute the basic principle of ion polymer actuators.

2.1. Composition

As mentioned in Section 1, normally, an IPMC consists of an ionomer membrane plated on both sides with metal electrodes and neutralized with the necessary amount of mobile ions and fixed counterions. Metal electrodes form the outermost layers, followed by the intermediate layer. The intermediate layer comprises of metal particles dispersed inside the polymer matrix, which contains the ionomer, the counter ions and solvent molecules inside the membrane as shown in **Figure 2**. Nafion by DuPont or Flemion by Asahi Glass are most used as ionomer. The differences between them are in the functional groups (sulfonate and carboxylate groups respective) and ion-exchange capacities. The chemical structure of Nafion and Flemion are shown in **Figure 2(a)**. The commonly used cations inside the membrane include the alkali metal cations, such as Li, Na, K, Rb and Cs while the solvent mainly refer to water and ionic liquid [21, 22]. For electrode layer, due to their corrosion resistance and high conductivity, platinum and gold are
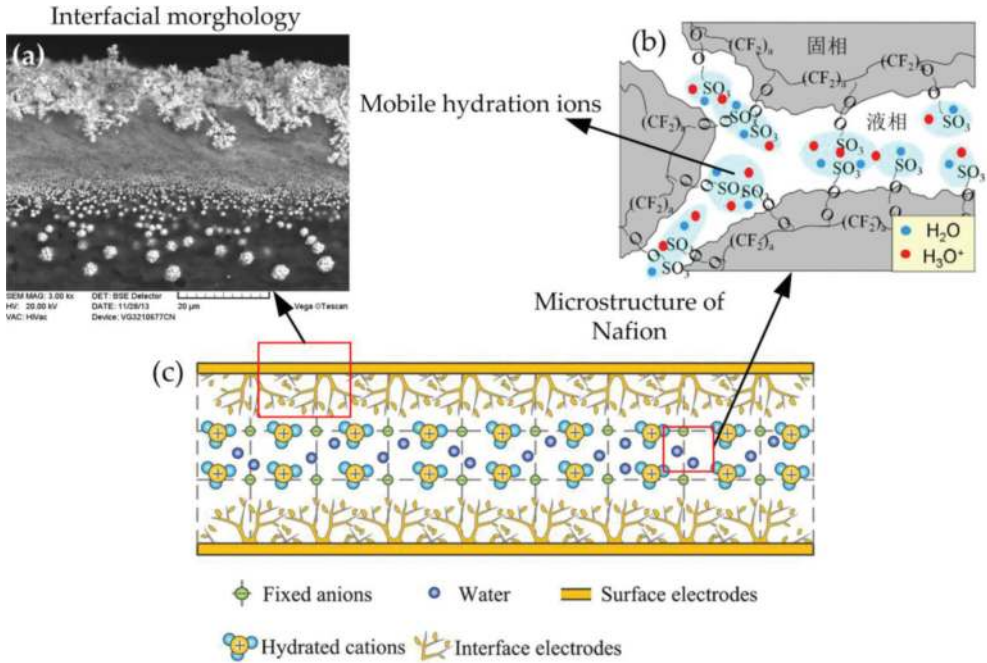
Interfacial morghology

Figure 2. Pd typed IPMC: (a) electrode interfacial morphology; (b) microstructure of Nafion; (c) schematic diagram of composition.

commonly used [1, 23]. In our lab, we developed palladium typed IPMC because of its relative low price and optimized its preparation process [17, 24].

Bucky gel actuators (BGAs) are composed by carbon nanotubes (CNTs), ionic liquid (IL), and base polymer (BP). Single-walled CNT (SWCNT) is one of good nanocarbons as conductive electrode material. Not only imidazolium-type ILs but also ammonium-type ILs can be used as electrolyte source. Polyvinylidene fluoride-co-hexafluoropropylene (PVDF-HFP) is used as a BP. BGAs have a three-layered structure as shown in **Figure 3**, that is, one electrolyte layer is laminated by two electrode layers. A gel like self-standing electrolyte film is made with IL and BP. Generally, the electrode films are made from CNTs, IL, and BP. Some additives such as conductive or non-conductive nanoparticles can be added in the electrode layers in order to tune the electrochemical and mechanical properties of electrode [25, 26].

In contrast to IPMC and BGA, we can see that they both have very similar structures, with the exception of the ingredient of the electrode layer and interlayer, separately. This, of course, will finally result in the difference in preparation process and electromechanical performance.

2.2. Bending mechanism

The working mechanism of IPMC can be explained through electromechanical transduction. When applying an electric field, the cations inside the base membrane move toward
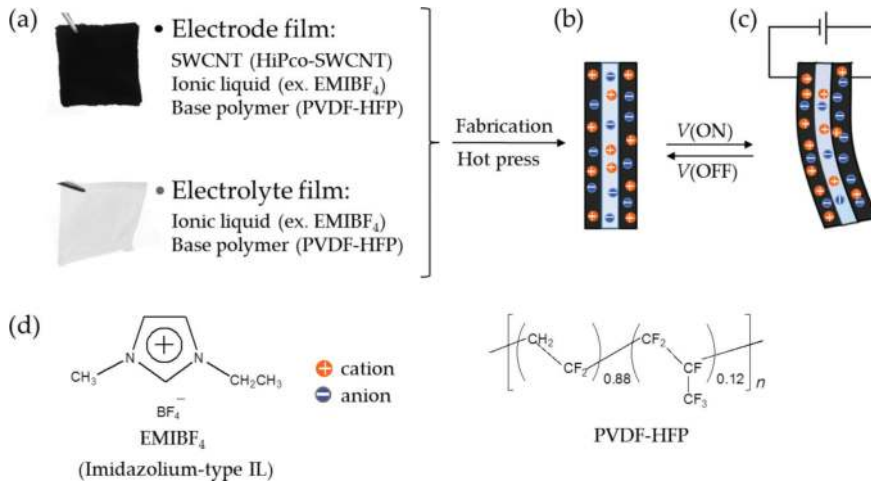
Figure 3. Components of electrode film and electrolyte film of bucky gel actuator (BGA) (a) Schematic representation of three-layered BGA (b) and the bending motion to the anode side (c) Chemical structure of imidazolium-type IL (EMIBF4) and base polymer (PVDF-HFP) (d).

the cathode with water molecules. The asymmetric distributions of the concentration of cations and water cause the IPMCs to swell near the cathode and generates extensional stress in the polymer, which causes the IPMC to swell near the cathode and shrink beside the anode. Finally, a bending motion is generated toward the anode [11]. Likewise, when an external stimuli was applied to the IPMC, the distributions of ions and water molecules inside IPMCs changes. Potential difference appears on both sides of the IPMC, which could be viewed as sensing signal. The properties of sensing and actuating of IPMC depend on the types of cation and solvent, surface resistant, interface morphology and temperature and humidity, etc.

In general, the current is generated by ion transport in BGAs and the three-layered BGAs show a bending motion to the anode side when voltages are applied. The electric charge is stored capacitively in BGAs during applying voltages [25]. This implies that our BGA is a capacitor. Baughman et al. reported SWCNT sheets (bucky papers) show the expansion and contraction (actuation) in aqueous electrolyte solution against a counter electrode [27]. They proposed the actuation mechanism in which C-C bond distance in SWCNT changes by charge injection originated from quantum and double-layer electrostatic effects. On the other hands, we consider the actuation mechanism of BGAs is due to C-C bond distance changing in CNTs [27, 28], volume change of the electrodes by sorption/desorption of ions [29], and electrostatic effect in the electrical double-layer [30]. Kiyohara and Asaka theoretically investigated the actuation mechanism of BGAs by a method of Monte Carlo simulation [31, 32]. We also studied the actuation mechanism of BGAs by a combination of symmetrical analysis, elasticity theory, and experimental results in the bulk scale [33]. As a result, it was found that the cathode expands and the anode contracts resulting in the bending motion of BGAs to the anode side.

3. Fabrication methods

3.1. IPMC

The current IPMC preparation technique involves two distinct steps: initial pretreatment, impregnation–reduction (IR) and chemical deposition. In our lab, we improve the technique by combining impregnation electroplating (IEP) [19]. The detailed process is as follows:

1) Nafion 117 was used as the interlayer roughened by sandblasting process. The diameter size of powders 200# is 0.0750 mm and the sandblasting time is 30 s. 2) Immerse the pre-treated Nafion in a 160 mL ammonia solution of [Pd (NH3)4]Cl2 with 140 mg Pd and 20 mL ammonia of 25% for 2 h with low-speed stirring. Then soak the pre-exchanged Nafion with the Pd complex cations in an alkaline solution of $NaBH_4$ (2–5%, PH > 13) under an ultrasonic environment at a continuous raising temperature (i.e. from 30 to 50°C). Repeat the first two steps for 3 times. 3) The pretreated Nafion membrane was soaked in Pd complex solution again for over 2 h and then placed in the apparatus to electroplate for over 30 s for both sides. Repeat the third step for 3 times. Immerse the IPMC in an aqueous solution of NaOH (0.1–0.5 mol/L) for 2 h.

3.2. BGA

A typical preparation method to fabricate BGAs is described below. The electrode film was obtained from SWCNT (HiPco–SWCNT, purified grade), PVDF-HFP (Kynar Flex®2801), and 1-ethyl-3-methylimidazolium tetrafluoroborate (EMIBF4) as an ionic liquid. 20 wt% of SWCNT, 32 wt% of PVDF-HFP, and 48 wt% of EMIBF4 were dissolved into 9 mL of N, N-dimethylacetamide (DMAC) and stirred for more than 1 day at room temperature, then sonicated for 24 hours in an ultrasonic bath. A gelatinous black solution was obtained after sonication. Obtained gelatinous solution was cast into a Teflon mold (25×25 mm^2) and dried on a hotplate at 50°C for 12 hours and dried DMAC furthermore at 80°C in vacuo for 3 days. As a result, a black self-standing electrode film was obtained. The electrolyte film was obtained from similar procedure. 50 wt% of PVDF-HFP and 50 wt% of EMIBF4 were mixed into the solvent mixture of 4-methyl-2-pentanone and propylene carbonate anhydrous and cast into the mold. The solvents were dried on a hot-plate then an opaque self-standing gel electrolyte was obtained. One electrolyte film was sandwiched by two electrode films with a hot-pressing technique to obtain the three-layered BGA. Super-growth SWCNT is also good nanocarbon for the electrode of BGAs [34]. The more detail fabrication process is described elsewhere [25, 26].

4. Electromechanical responses

To evaluate the effect of parameters, the responses of IPMC, mainly including current and deformation, are measured in fully hydrated state. The performances of strip sample were tested for comparison. **Figure 4** shows the testing schematic. The strip sample with 40 mm in length and 5 mm in width is clamped by two copper disks. The displacement at the point 25 mm away from the fixed point is measured by a laser displacement sensor (Keyence, LK-G80). The applied voltage and current are simultaneously measured. The tip displacement w of samples can be calculated from the measured displacement δ by the following Eq. (1).

$$w = 2R \sin^2\left(\frac{l}{2R}\right), \tag{1}$$

where l is the length of the free part of IPMC strip. The radius of curvature R is evaluated from the measured displacement by the following Eq. (2).

$$\frac{1}{R} = 2\delta/(d^2 + \delta^2) \tag{2}$$

where d is the distance between the measuring point and the fixed point.

The currents and deformations under DC voltage were measured more than 20 s. The voltage range was set from 0.5 to 1.7 V with an interval of 0.3 V. For the electrochemical system composed of water, palladium, Nafion, and Na + cations, the electrolytic voltage of water is 1.75 V even higher [35]. So the voltages higher than 1.7 V were not employed in order to avoid the electrolysis process of water. To facilitate the analysis, the averages and errors of the peak currents and maximum deformations of the samples, testing three times for each sample, were extracted and recorded as shown in **Figure 5**. It can be observed that the peak currents increase with the applied voltage increasing (**Figure 5(a)**). Under the voltage of 2 V, the current response fluctuates in some degree due to the electrolysis of water. From **Figure 5(b)**, the maximum displacements of sample exhibit significant differences. With the applied voltages in an increase, the maximum displacements are increased.

To further investigate the relationship between the electrode morphologies, physical and electrical parameters and the electromechanical responses, an electrical component is introduced to explain the deformation behavior of IPMC as shown in **Figure 6**.
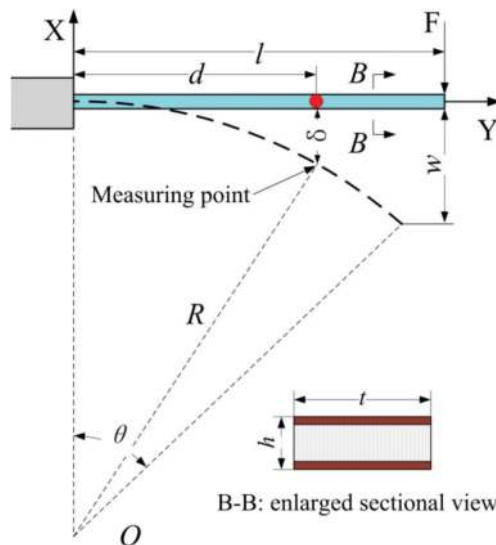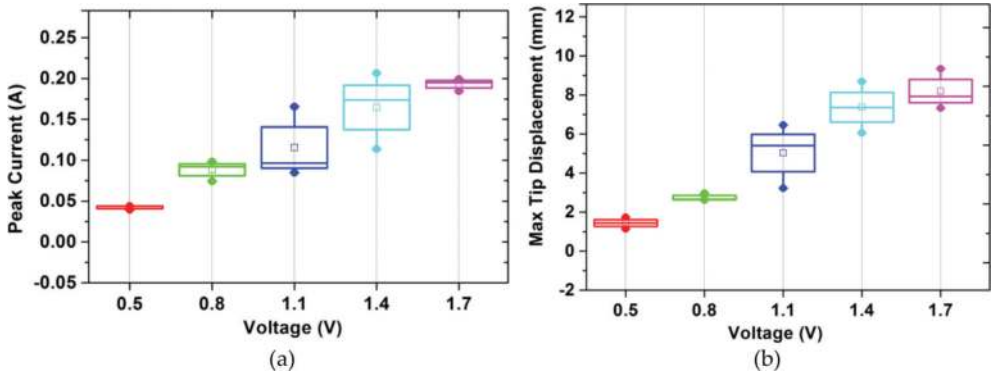

Figure 4. Schematic of the bending deformation.

Figure 5. (a). Peak current of IPMC strip under different voltage; (b) Maximum displacements of samples versus voltages.
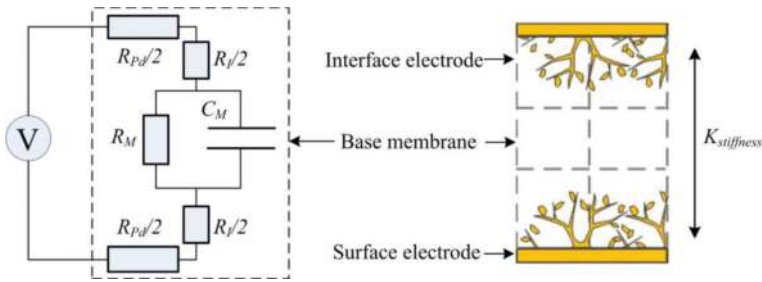

Figure 6. Equivalent circuit of IPMC.

The interlayer of IPMC can be viewed as an ion conductive material and modeled by a capacitor and a resistor in parallel. The electrode can be modeled by two resistors. Then the peak current i_{peak} (total current) can be figured out by Eq. (3). The first item of the Eq. (3) describes the steady-state current from the resistance components, while the second item reflects the transient current from the capacitive element. Eq. (4) shows the qualitative relations between deformation, peak current and bending stiffness based on experimental test.

$$i_{peak} = \frac{U}{R_{Pd} + R_m} + \frac{\varepsilon S_1}{4kd} \cdot \frac{dU}{dt}, \tag{3}$$

$$D \sim \frac{i_{peak}}{K_{stiffness}}, \tag{4}$$

where U, R_{Pd}, S_1, D and $K_{stiffness}$ represent applied voltage, surface resistance, area of interface electrode, deformation and bending stiffness, respectively. Other parameters, such as R_m, ε, π, k and d, are considered to be constants.

It shows that the peak current depends on the electrode resistance, surface resistance, membrane resistance and the area of interface electrode closely related to dielectric modulus under

the condition of constant voltage. Eq. (3) and (4) can be employed to interpret the deformation behaviors of IPMC. From the perspective of the fabrication process, different fabrication process will exert an important effect on the surface resistances of the samples. Roughening increases the surface resistance while chemical plating can reduce it. Meanwhile, the decrease of surface resistance largely increases the bending stiffness. Although the bending stiffness does not contribute to peak current directly, it is also a key factor to affect the deformation of IPMC as shown in Eq. (3). So it is necessary to optimize the roughening process and chemical plating process. The impregnation-reduction process mainly forms a penetration electrode to increase the area of interface electrode. But it is difficult to further improve the interface due to the blocking effect of previous plated layer.

As we described before, the capacitive current is generated in BGAs during applying voltages. This means that the electrolyte (ionic liquid (IL)) plays a very important role for the actuation of BGAs. So, we studied the influence of ILs on the actuation mechanism of BGAs. We investigated the electrochemical and electromechanical properties of BGAs by using seven kinds of ILs [36]. The chemical structures of ILs are shown in **Table 1**. Some physicochemical properties, such as melting point (T_{mp}), viscosity (η) at 25° C, and electric conductivity (κ) are also summarized in **Table 1**, especially for imidazolium-type ILs [37]. We measured the displacement of bending by a laser displacement meter at different frequencies of applied voltages in order to investigate actuation properties of BGAs. The three-layered BGA sample (normally, the actuator sample has a size of 1 (width) x 10 mm (length)) was clipped by two gold current collectors to apply voltages. Then, alternative voltages were applied to actuator sample. A Potentio/Galvanostat with a wave generator was used to apply voltages. The voltage, current, and displacement were simultaneously monitored by an oscilloscope. The detail experimental setup is described elsewhere [25, 38].
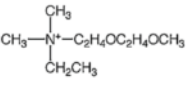
Ionic liquid		Cation		Anion	T_{mp} (°C)	η (cP) at 25 °C	κ (mS cm^{-1})
Imidazolium type IL	EMIBF$_4$		R= C$_2$H$_5$		14.6	31.8	13.6
	BMIBF$_4$		R= C$_4$H$_9$	BF$_4$$^-$	−71	118.3	3.43
	HMIBF$_4$		R= C$_6$H$_{13}$		−82	223.8	1.04
	OMIBF$_4$		R= C$_8$H$_{17}$		−80	422.0	0.576
	EMITFSI			(CF$_3$SO$_2$)$_2$N$^-$	−16	28.0	8.40
Ammonium type IL	A−3			BF$_4$$^-$			
	A−4			(CF$_3$SO$_2$)$_2$N$^-$			

Table 1. Chemical structure and physicochemical property of IL [37].

The observed displacement (δ) was converted to the strain difference (ε) between the two electrodes of BGAs in order to normalize the size differences of BGAs by using the following equation on the assumption that there is no distortion of the cross-sections in the actuator during bending.

$$\varepsilon = 2D\delta/(L2 + \delta 2) \tag{5}$$

where D is the thickness of actuator sample and L is the free length of actuator sample from the fixed end of gold current collectors.

The frequency dependence of strain (ε) for BGAs including seven kinds of ILs is shown in **Figure 7**. The BGA with EMIBF4 as an electrolyte shows the best actuation (strain) in all the frequency range. The strain becomes worse with increasing the length of alkyl chain in the imidazolium-cation. This is the reason why the ionic conductivity decreases with increasing the length of alkyl chain related to increasing the viscosity. The frequency dependence of strain can be successfully fit to an electrochemical kinetic model (a double-layer charging kinetic model). In this model, the electrode of BGA is fully charged at low frequencies of applied voltage. However, there is not enough time to be fully charged for the electrode at higher frequencies. In other words, the stored charge (Q) decreases with increasing the frequencies of applied voltage. In this consideration, the strain (ε) is proportional to the stored charge (Q). A simple equivalent circuit model was used to make the electrochemical kinetic model as shown in **Figure 8**. The double-layer capacitance of each electrode ($C1$) is replaced by the capacitance (C); $C = C1/2$. R is resistance of ionic gel electrolyte. R is calculated from the ionic conductivity κ (=thickness/R × area). The stored charge $Q(f)$ at a frequency (f Hz) is represented by the following equation:

$$Q(f)/Q0 = 1 - 4CRf(1 - \exp(-1/4CRf)) \tag{6}$$

where $Q0$ is the stored charge at a limit of low frequency. And the strain ($\varepsilon(f)$) is given by following equation:

$$\varepsilon(f) = \varepsilon 0 Q(f)/Q0 \tag{7}$$

where $\varepsilon 0$ is the strain at a limit of low frequency.

The obtained parameters such as the double layer capacitance of the electrode (C), the ionic conductivity of the ionic gel electrolyte (κ), the calculated resistance of the ionic electrolyte (R), the strain at a limit of low frequency ($\varepsilon 0$), and the time constant (CR) are summarized in **Table 2**. Base on the equivalent circuit model analysis, it was found that the frequency dependence of actuation of BGAs is depended on the electrochemical time constant (CR) that is mainly related to the ionic conductivity. Furthermore, the actuation of BGAs is affected by the size difference between cation and anion included as an internal electrolyte because the volume changes of cathode and anode are caused by the sorption/desorption of cations and anions. More detail studies on the impedance analysis for the porous structure in the electrode of BGAs [39] and further studies on electrochemical energy and power density of BGAs [40] were reported by Randriamahazaka and Asaka et al. It was found that BGA behaves as supercapacitors and the electrochemical energy
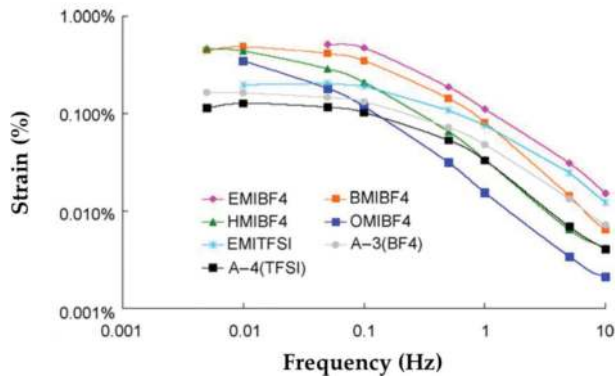
Figure 7. Frequency dependence of strain difference (e) for BGAs with seven kinds of ILs (reproduced with permission [36]).
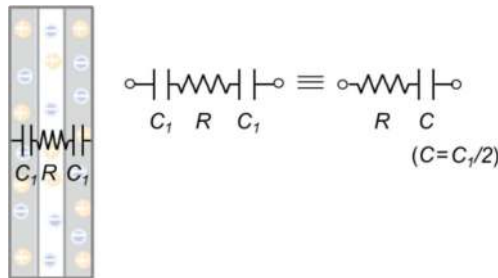

Figure 8. Equivalent circuit model of BGA.

Ionic liquid	C_{SWCNT} (F g^{-1})	C (F cm^{-2})	κ (mS cm^{-1})	R (Ω cm^2)	ε_0 (%)	CR (s)
EMIBF$_4$	45.5	0.0312	1.71	1.17	0.53	0.0365
BMIBF$_4$	45.3	0.0338	0.312	6.41	0.45	0.217
HMIBF$_4$	44.8	0.0286	0.134	14.9	0.48	0.426
OMIBF$_4$	44.6	0.0286	0.014	143	0.60	4.09
EMITFSI	49.2	0.0338	1.33	1.50	0.21	0.0507
A$-$3	35.4	0.0286	0.393	5.09	0.17	0.146
A$-$4	41.6	0.0286	0.729	2.74	0.13	0.0784

Table 2. Gravimetric capacitance of SWCNT(CSWCNT) and double-layer capacitance per electrode area (C) of BGA electrode, ionic conductivity (κ) and ionic resistance (R) of ionic gel electrolyte, strain difference at a limit of low frequency (ε0) and time constant (CR) (reproduced with permission [36]).

densities of BGAs are of the same order of magnitude as those of natural muscles. Similar ionic polymer actuators with carbonaceous electrodes are introduced in a review paper by Asaka et al. [41].

5. Typical applications

Ionic polymer actuators have been expected to be used for some practical applications such as active microcatheters, micropumps, tactile displays, biomimetic microrobots, and so on [42, 43]. First commercial production with ionic EAP was produced by a Japanese company (Eamex Co.) in 2002 ([42] p. 2). They produced a fish robot which has a caudal fin made with ionic EAP. They can control the movement of the caudal fin by electromagnetic induction (wireless control).

Here, we introduce three examples of our application trials with IPMC and BGAs.

First sample is the prototype of developed micropump using inner petal-shaped IPMC actuator as shown in **Figure 9**. Micropumps capable of providing an appropriate flow rate and a reasonable back pressure are usually inevitable requirements for a self-contained micro-fluidic system. Since this is a prototype only, the pump was not made to be very small. The overall size is 70 × 40 × 15 mm (length × width × height). The pump chamber is a 15 mm in diameter, 2 mm in depth. It should be noted that, we only tested inner petal-shaped IPMC actuator with a diameter of 15 mm. The actuator used in this prototype is a Nafion 117-based IPMC actuator. A pair of copper plates as electrodes was used to clamp the two sides of the IPMC actuator, providing the stimulus electrical signal. In order to evaluate the performance of micropump, we carry out the experiment of the flow rate and the back pressure measurement in 1 Hz sine voltage input by changing the voltage amplitude from 0.5 to 3 V by the interval of 0.5 V. The experimental results show that the flow rate from 162 to 1611 μL/min can be obtained by changing the voltage amplitude from 0.5 to 3 V, respectively. And the back pressure on the micropump can be as high as 71 mm-H2O under the condition of 1 Hz and 3 V sine voltage input.

Second example is an ultra-thin and ultra-light refreshable Braille display with BGAs [41, 44]. There are more than 100 million visually impaired people in the world. This means there are a huge number of people who cannot access the internet because most information in the internet are shown with words and photos on the liquid crystal displays of mobile phones, laptop computers, and other tablet tools. Currently, the refreshable Braille displays with inorganic piezoelectric actuators are commercially available but they are not suitable for the mobile use
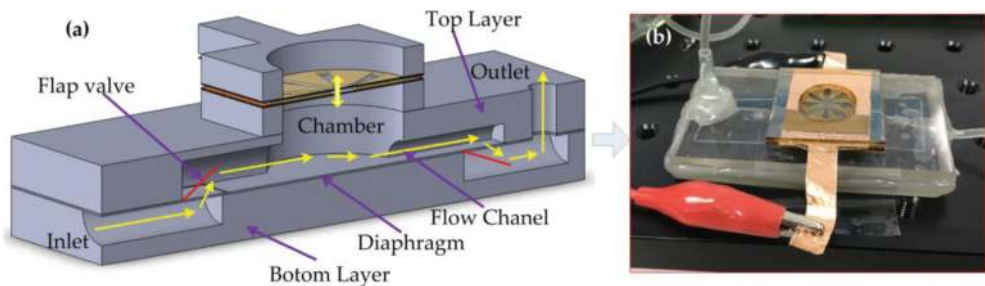

Figure 9. The principle (a) and appearance (b) of the fabricated micropump.

because they are heavy (~kg) and large (266 (length) × 129 (width) × 40 mm (thickness) for a 32 Braille characters display). So, we had a motivation to produce an ultra-light and ultra-thin Braille display by using BGAs. The developed prototype Braille display with BGAs is shown in **Figure 10** which has a size of 65 (length) × 30 (width) × 3 mm (thickness) with 6 refreshable Braille characters and the weight is only 5 g. This prototype Braille display was produce by collaborations with ALPS Electric Co., Ltd. Our Braille display was readable for most of visually impaired people but not readable for some visually impaired people who are not used to use Braille display. This is the reason why the dot force is not enough compared to commercial Braille displays. Improving the force and the durability is now in progress.

Third example is the application for micropipette and micropump. Recently, micropipettes and micropumps have been receiving a lot of attention for the microfluidic point-of-care (POC) diagnostic devices. So, we are willing to test the potential of BGAs as a micropipette. This project has been done by collaborations with Fraunhofer IPA (Stuttgart, Germany) [45]. A BGA (black square film) was set into the printed circuit boards (PCBs) to apply voltages as shown in **Figure 11**. The pipette has a channel tip which has a size of 1 × 1 × 10 mm to suck and release liquid. The BGA showed an up-and-down motion in the PCBs like a diaphragm pump and can dispense *ca*. 10–20 μL liquid. Furthermore, Goya et al. developed a BGA micropipette system equipped with commercially available two- and
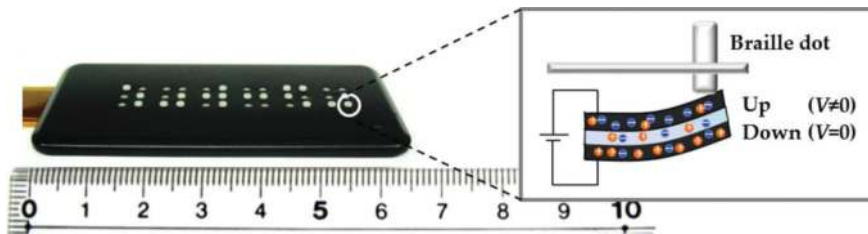

Figure 10. A photo of prototype braille display with BGAs and an illustration of movement of a braille dot by the bending of BGA.
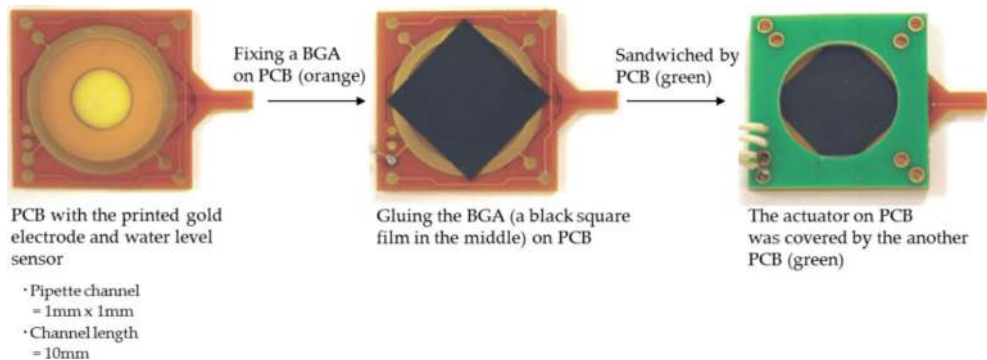

Figure 11. A photo of prototype micropipette with BGAs. A black square BGA are set between two PCBs.

three-way solenoid valves [46]. In this system, the three-way valve and a particular two-way valve are open during the BGA shows upward motion (during sucking water). They were successful to dispense *ca*. 20 μL water droplet within 2% of relative standard deviation. We hope that our BGAs will be practically appreciable for some medical and medical welfare devices in the near future.

6. Conclusions

Ionic polymer actuator is a class of functional polymers that has great potential for application in soft robotics and micro-devices. In this chapter, two representative ionic polymer actuators are introduced: IPMC and BGA. Some fundamental characteristics and properties of the ionic polymer actuator have been clarified, and some recent applications in the micro pump, braille display and micropipette of IPMC and BGA as soft actuators have been presented.

Acknowledgements

Note

The authors contributed equally to this work.

Author details

Yanjie Wang[1]* and Takushi Sugino[2]

*Address all correspondence to: yjwang@hhu.edu.cn

1 School of Mechanical and Electrical Engineering, HoHai University, Changzhou, China

2 Inorganic Functional Materials Research Institute, National Institute of Advanced Industrial Science and Technology (AIST), Ikeda, Osaka, Japan

References

[1] Tiwari R, Garcia E. The state of understanding of ionic polymer metal composite architecture: A review. Smart Materials and Structures. 2011;**20**(8):083001

[2] Jo C, Pugal D, Oh IK, et al. Recent advances in ionic polymer–metal composite actuators and their modeling and applications. Progress in Polymer Science. 2013;**38**(7):1037-1066

[3] Wang Y, Chen H, Liu J, et al. Aided manufacturing techniques and applications in optics and manipulation for ionic polymer-metal composites as soft sensors and actuators. Journal of Polymer Engineering. 2015;**35**(7):611-626

[4] Adolf D, Shahinpoor M, Segalman D, Witkowski W. Electrically Controlled Polymeric Gel Actuators, US Patent Number 5250167, October 1993

[5] Oguro K, Takenaka H, Kawami Y. Actuator Element. US Patent Office, US patent no. 5268082, Issued December 7, 1993

[6] Shahinpoor M. Continuum electromechanics of ionic polymeric gels as artificial muscles for robotic applications. Smart Materials and Structures. 1994;**3**(3):367

[7] Shahinpoor M. Micro-electro-mechanics of ionic polymeric gels as electrically controllable artificial muscles. Journal of Intelligent Material Systems and Structures. 1995;**6**(3):307-314

[8] Salehpoor K, Shahinpoor M, Mojarrad M. Linear and platform type robotic actuators made from ion-exchange membrane-metal composites. Proceedings of SPIE Smart Material Structure. 1997;**3040**:192-198

[9] Tadokoro S, Yamagami S, Takamori T, et al. Modeling of Nafion-Pt composite actuators (ICPF) by ionic motion[C]//smart structures and materials 2000: Electroactive polymer actuators and devices (EAPAD). International Society for Optics and Photonics. 2000;**3987**:92-103

[10] Shahinpoor M, Bar-Cohen Y, Simpson JO, et al. Ionic polymer-metal composites (IPMCs) as biomimetic sensors, actuators and artificial muscles-a review. Smart Materials and Structures. 1998;**7**(6):R15

[11] De Gennes PG, Okumura K, Shahinpoor M, et al. Mechanoelectric effects in ionic gels. EPL (Europhysics Letters). 2000;**50**(4):513

[12] Newbury KM, Leo DJ. Linear electromechanical model of ionic polymer transducers-part I: Model development. Journal of Intelligent Material Systems and Structures. 2003;**14**(6):333-342

[13] Newbury KM, Leo DJ. Linear electromechanical model of ionic polymer transducers-part II: Experimental validation. Journal of Intelligent Material Systems and Structures. 2003;**14**(6):343-357

[14] Nemat-Nasser S, Li JY. Electromechanical response of ionic polymer-metal composites. Journal of Applied Physics. 2000;**87**(7):3321-3331

[15] Zhu Z, Asaka K, Chang L, et al. Multiphysics of ionic polymer–metal composite actuator. Journal of Applied Physics. 2013;**114**(8) 084902

[16] Zhu Z, Wang Y, Liu Y, et al. Application-oriented simplification of actuation mechanism and physical model for ionic polymer-metal composites. Journal of Applied Physics. 2016;**120**(3) 034901

[17] Chang L, Chen H, Zhu Z, et al. Manufacturing process and electrode properties of palladium-electroded ionic polymer–metal composite. Smart Materials and Structures. 2012;**21**(6) 065018

[18] Chung CK, Fung PK, Hong YZ, et al. A novel fabrication of ionic polymer-metal composites (IPMC) actuator with silver nano-powders. Sensors and Actuators B: Chemical. 2006;**117**(2):367-375

[19] Wang Y, Liu J, Zhu Y, et al. Formation and characterization of dendritic interfacial electrodes inside an Ionomer. ACS Applied Materials & Interfaces. 2017;**9**(36):30258-30262

[20] Fukushima T, Asaka K, Kosaka A, et al. Fully plastic actuator through layer-by-layer casting with ionic-liquid-based Bucky gel. Angewandte Chemie International Edition. 2005;**44**(16):2410-2413

[21] Nemat-Nasser S, Wu Y. Comparative experimental study of ionic polymer–metal composites with different backbone ionomers and in various cation forms. Journal of Applied Physics. 2003;**93**(9):5255-5267

[22] Zhu Z, Chang L, Takagi K, et al. Water content criterion for relaxation deformation of Nafion based ionic polymer metal composites doped with alkali cations. Applied Physics Letters. 2014;**105**(5) 054103

[23] Wang Y, Chen H, Wang Y, et al. Effect of dehydration on the mechanical and physicochemical properties of gold-and palladium-ionomeric polymer-metal composite (IPMC) actuators. Electrochimica Acta. 2014;**129**:450-458

[24] Wang Y, Zhu Z, Liu J, et al. Effects of surface roughening of Nafion 117 on the mechanical and physicochemical properties of ionic polymer–metal composite (IPMC) actuators. Smart Materials and Structures. 2016;**25**(8) 085012

[25] Sugino T, Kiyohara K, Takeuchi I, Mukai K, Asaka K. Actuator properties of the complexes composed by carbon nanotube and ionic liquid: The effect of additives. Sensors and Actuators B. 2009;**141**:179-186. DOI: 10.1016/j.snb.2009.06.002

[26] Sugino T, Kiyohara K, Takeuchi I, Mukai K, Asaka K. Improving the actuating response of carbon anotube/ionic liquid composites by the addition of conductive nanoparticles. Carbon. 2011;**49**:3560-3570. DOI: 10.1016/j.carbon.2011.04.056

[27] Baughman RH, Cui C, Zakhidov AA, Iqbal Z, Barisci JN, Spinks GM, Wallace GG, Mazzordi A, Rossi DD, Rinzler AG, Jaschinski O, Roth S, Kertesz M. Carbon nanotube actuators. Science. 1999;**284**:1340-1344. DOI: 10.1126/science.284.5418.1340

[28] Chan CT, Kamitakahara WA, Ho KM. Charge-transfer effects in graphite intercalates: Ab initio calculations and neutron-diffraction experiment. Physical Review Letters. 1987;**58**:1528-1531. DOI: 10.1103/PhysRevLett.58.1528

[29] Hahn M, Barbieri O, Campana FP, Kötz R, Gallay R. Carbon based double layer capacitors with aprotic electrolyte solutions: The possible role of intercalation/insertion processes. Applied Physics A: Materials Science & Processing. 2006;**82**:633-638. DOI: 10.1007/s00339-005-3403-1

[30] Oren Y, Glatt I, Livnat A, Kafri O, Soffer A. The electrical double layer charge and associated dimensional changes of high surface area electrodes as detected by moire deflectometry. Journal of Electroanalytical Chemistry. 1985;**187**:59-71. DOI: 10.1016/0368-1874(85)85575-1

[31] Kiyohara K, Asaka K. Monte Carlo simulation of electrolytes in the constant voltage ensemble. The Journal of Chemical Physics. 2007;**126**:214704-214714. DOI: 10.1063/1.2736371

[32] Kiyohara K, Asaka K. Monte Carlo simulation of porous electrodes in the constant voltage ensemble. Journal of Physical Chemistry C. 2007;**111**:15903-15909. DOI: 10.1021/jp0736589

[33] Kiyohara K, Sugino T, Takeuchi I, Mukai K, Asaka K. Expansion and contraction of polymer electrodes under applied voltage. Journal of Applied Physics. 2009;**105**:063506-1-8 [Erratum: J Appl Phys 2009;105:119902-1] DOI: 10.1063/1.3078031 [Erratum: DOI: 10.1063/1.3141728]

[34] Hata K, Futaba DN, Mizuno K, Namai T, Yumura M, Iijima S. Water-assisted highly efficient synthesis of impurity-free single walled carbon nanotubes. Science. 2004;**306**:1362-1364. DOI: 10.1126/science.1104962

[35] Zoulias E, Varkaraki E, Lymberopoulos N, Christodoulou CN, Karagiorgis GN. A review on water electrolysis. TCJST. 2004;**4**(2):41-71

[36] Takeuchi I, Asaka K, Kiyohara K, Sugino T, Terasawa N, Mukai K, Fukushima T, Aida T. Electromechanical behavior of fully plastic actuators based on buckey gel containing various internal inonic liquids. Electrochimica Acta. 2009;**54**:1762-1768. DOI: 10.1016/j.electacta.2008.10.007

[37] Ohno H, editor. Ionic Liquid II: Marvelous Developments and Colorful Near Future. Japan: CMC; 2006. 299 p. ISBN: 4-88231-557-2

[38] Takeuchi I, Asaka K, Kiyohara K, Sugino T, Terasawa N, Mukai K, Shiraishi S. Electromechanical behavior of a fully plastic actuator based on dispersed nano-carbon/ionic-liquid-gel electrodes. Carbon. 2009;**47**:1373-1380. DOI: 10.1016/j.carbon.2009.01.029

[39] Takeuchi I, Asaka K, Kiyohara K, Sugino T, Mukai K, Randriamahazaka H. Electrochemical impedance spectroscopy and electromechanical behavior of bucky-gel actuators containing ionic liquids. Journal of Physical Chemistry C. 2010;**114**:14627-14634. DOI: 10.1021/jp1018185

[40] Randriamahazaka H, Asaka K. Electrochemical analysis by means of complex capacitance of bucky-gel actuators based on single-walled carbon nanotubes and an ionic liquid. Journal of Physical Chemistry C. 2010;**114**:17982-17988. DOI: 10.1021/jp106232s

[41] Asaka K, Mukai K, Sugino T, Kiyohara K. Ionic electroactive polymer actuators based on nano-carbon electrodes. Polymer International. 2013;**62**:1263-1270. DOI: 10.1002/pi.4562

[42] Bar-Cohen Y, editor. Electroactive Polymer (EAP) Actuators as Artificial Muscles: Reality, Potential, and Challenges. 2nd ed. Washington: SPIE; 2004. 765 p. DOI: 10.1117/3.547465

[43] Carpi F, Smela E, editors. Biomedical Applications of Electroactive Polymer Actuators. West Sussex: Wiley; 2009. 476 p. DOI: 10.1002/9780470744697

[44] Takahashi I, Takatsuka T, Abe M. Application of nano-carbon actuator to braille display. In: Asaka K, Okuzaki H, editors. Soft Actuators: Materials, Modeling, Applications, and Future Perspectives. Springer Japan: Springer; 2014. pp. 371-384. DOI: 10.1007/978-4-431-54767-9.ch27

[45] Addinall R. Sugino T, Neuhaus R, Kosidlo U, Tonner F, Glanz C, Kolaric I, Bauerhansl T, Asaka K. Integration of CNT-based actuators for bio-medical applications-example printed circuit board CNT actuator pipette. In: Proceedings of 2014 IEEE/ASME international conference on advanced intelligent mechatronics (AIM); 8-11 July 2014; Besacon. France: IEEE; 2014. p. 1436-1441

[46] Goya K, Fuchiwaki Y, Tanaka M, Addinall R, Ooie T, Sugino T, Asaka K. A micropipette system based on low driving voltage carbon nanotube actuator. Microsystem Technologies. 2017;**23**:2657-2661. DOI: 10.1007/s00542-016-2943-y